Journal of Alloys and Compounds 731 (2018) 1146–1150

Contents lists available at ScienceDirect

Journal of Alloys and Compounds

journal homepage: http://www.elsevier.com/locate/jalcom

Effect of W addition on the glass forming ability and mechanical properties of Fe-based metallic glass

Dan-dan Liang [a], Xian-shun Wei [a, *], Chun-tao Chang [b, c, **], Jia-wei Li [b, c], Xin-min Wang [b, c], Jun Shen [a]

[a] School of Materials Science and Engineering, Tongji University, 4800 Caoan Road, Shanghai, 201804, China
[b] Key Laboratory of Magnetic Materials and Devices, Ningbo Institute of Materials Technology and Engineering, Chinese Academy of Sciences, Ningbo, Zhejiang, 315201, China
[c] Zhejiang Province Key Laboratory of Magnetic Materials and Application Technology, Ningbo Institute of Materials Technology and Engineering, Chinese Academy of Sciences, Ningbo, 315201, China

ARTICLE INFO

Article history:
Received 14 June 2017
Received in revised form
11 October 2017
Accepted 14 October 2017
Available online 16 October 2017

Keywords:
Metallic glasses
W addition
Glass forming ability
Microhardness
Compressive strength

ABSTRACT

The effects of refractory element W addition on the glass forming ability (GFA) and mechanical properties of $Fe_{47-x}Cr_{20}Mo_{10}W_xC_{15}B_6Y_2$ ($x = 0$, 2, 4, 6 at. %) alloys were investigated. The supercooled liquid region ΔT_x ($T_x - T_g$) and criterion γ [$T_x/(T_g + T_l)$] of $Fe_{47-x}Cr_{20}Mo_{10}W_xC_{15}B_6Y_2$ alloys increased to 62 K and 0.390, respectively, when x increased to 4 at. %. An appropriate substitution of Fe by W (4 at. %) significantly improved the GFA by suppressing the formation of the $Fe_{23}B_6$ phase. The GFA and thermal stability decreased when x increased to 6 at. %. The $Fe_{43}Cr_{20}Mo_{10}W_4C_{15}B_6Y_2$ bulk metallic glass (BMG) rod with an 8 mm diameter could be fabricated by using commercial purity materials. The addition of the refractory W element could also enhance the microhardness, compressive strength and plasticity of $Fe_{47-x}Cr_{20}Mo_{10}W_xC_{15}B_6Y_2$ BMGs. The $Fe_{41}Cr_{20}Mo_{10}W_6C_{15}B_6Y_2$ BMG exhibited high compressive strength of 4.12 GPa and microhardness of 1267 HV.

1. Introduction

Bulk metallic glasses (BMGs) have been studied extensively for their unique properties, such as high strength and hardness, as well as excellent corrosion and wear resistance [1–6]. Among the metallic glass alloy systems, Fe-based BMGs have been widely investigated because of the abundant natural resources of the Fe element and the unique combination of superior physical and mechanical properties [7]. However, the glass forming ability (GFA) insufficiency of Fe-based BMGs has limited their engineering application as structural materials. Previous studies have reported that minor alloying is an effective approach to improve GFA by changing the atomic radius ratio and degree of mixing enthalpy [8,9]. Recently, non-ferromagnetic Fe-Cr-Mo-C-B-Y/Ln BMGs have been developed [10–15]. Many investigations have been carried out to improve the GFA and other properties of non-ferromagnetic Fe-based BMGs by minor alloying [16,17].

The addition of minor refractory elements (e.g., Mo, W, and Nb) to Fe-based BMGs can cause a significant atom size difference and beneficial effect on the GFA [18]. The refractory elements can also affect other properties, such as the melting temperature, high-temperature strength, and corrosion resistance; hence, the minor addition of refractory elements can tailor the mechanical property and other properties of Fe-based BMGs. The appropriate Mo addition to Fe-based BMGs can improve their GFA [19,20]. Studies about Nb addition on the GFA and thermal properties of Fe-based BMGs have also been reported [21,22]. One study reported that the mechanical strength could be ameliorated through the addition of the Nb element by increasing the structure packing density [23]. Using Mo and W elements to substitute Nb could deteriorate the GFA in Fe-Co-based BMGs [24]. Adding the W element in magnetic Fe-Y-B BMG could optimize the GFA and magnetic properties [25]. Unlike Mo or Nb element, the effect mechanism of the W element on the GFA and other properties of Fe-based BMGs remains unclear and has not been systematically discussed.

* Corresponding author. Tel.: +86 21 69581009.
** Corresponding author.
E-mail addresses: weixianshun@tongji.edu.cn (X.-s. Wei), ctchang@nimte.ac.cn (C.-t. Chang).

https://doi.org/10.1016/j.jallcom.2017.10.104
0925-8388/

This study investigates the effect of W element addition on the Fe-Cr-Mo-C-B-Y alloy system, which can be used to fabricate a new Fe-based metallic glass alloy with a highly stabile amorphous phase against crystallization and high mechanical properties.

2. Experimental

Fe-based alloys with nominal compositions $Fe_{47-x}Cr_{20}Mo_{10}W_xC_{15}B_6Y_2$ ($x = 0, 2, 4, 6$ at. %) were prepared by arc melting the mixture of commercial purity elements Fe (99.7 wt. %), Cr (99.98 wt. %), Mo (99.9 wt. %), C (99.999 wt. %), W (99. 5 wt. %), Y (99.6 wt. %), and pre-alloyed FeB (99.38 wt. %) in a Ti-gettered argon atmosphere. Each alloy ingot was remelted at least four times to obtain compositional homogeneity. Rod samples with different diameters were fabricated by drop casting the melts into a copper mold. The corresponding amorphous ribbons with 1 mm to 1.2 mm width and approximately 40 μm thickness were produced by the single roller melt-spinning method at a wheel speed of 35 m/s under argon atmosphere.

The structure of the as-cast Fe-based BMGs alloys was examined by an X-ray diffractometer (XRD) utilizing Cu K_α radiation. A thermal stability test of the amorphous melt-ribbon was conducted by using a NETZSCH 404 differential scanning calorimeter (DSC) instrument with a heating rate of 20 K/min.

The microstructure of as-cast alloys was characterized by a transmission electron microscopy (TEM, JEM-2100F) that was operated at a voltage of 200 kV. TEM foils were prepared by ion-milling with a Gatan 695 precision ion polishing system to decrease the possible thermal damage on the structure of TEM samples. The ion milling was operated at 3.5 keV with a milling angle of 6°. The microhardness of cylindrical specimens with diameter of 2 mm was examined by utilizing an HVS-1000A hardness tester with a load of 300 g. At least 20 indents were performed for each alloy. Indentation fracture toughness tests were performed with a load of 1000 g. The as-cast specimens with a diameter of 2 mm and length of 4 mm were tested under a quasi-static compressive condition with a strain rate of 5×10^{-4} s^{-1} utilizing a UTM5105 universal mechanical test machine at room temperature. Three compressive tests were performed for each alloy. The fracture morphology were analyzed by a scanning electron microscope (SEM, FEI Nova Nano 450).

3. Results and discussion

The XRD pattern of the as-cast $Fe_{47}Cr_{20}Mo_{10}C_{15}B_6Y_2$ ($x = 0$ at. %) sample with a diameter of 5 mm was presented in Fig. 1. The broad halo peak demonstrates that the $Fe_{47}Cr_{20}Mo_{10}C_{15}B_6Y_2$ alloy structure is a fully amorphous phase. The XRD pattern of the $Fe_{47}Cr_{20}Mo_{10}C_{15}B_6Y_2$ sample with a diameter of 6 mm shows several tiny peaks, which are identified as a $Fe_{23}B_6$ crystalline phase. All XRD patterns of the $Fe_{47-x}Cr_{20}Mo_{10}W_xC_{15}B_6Y_2$ ($x = 2, 4, 6$ at. %) samples with a diameter of 6 mm represent fully amorphous structures. Further increasing the diameter to 8 mm results in the appearance of several crystalline phases for the alloys with $x = 2$ at. % and $x = 6$ at. %. The tiny crystalline peaks correspond to the $Fe_{23}B_6$ crystalline phase for the alloy with $x = 2$ at. %. The sharp diffraction peaks correspond to the $Fe_{23}(B, C)_6$ and $Fe_3W_3(B, C)$ phases for the alloy with $x = 6$ at. %. When heating ternary Fe-W-B amorphous alloys above the crystallization temperature, the $Fe_3W_3(B, C)$-type crystal phase is also generated [26]. For the alloy with $x = 4$ at. %, the XRD pattern shows a fully amorphous structure for the sample with a diameter of 8 mm. The XRD results imply that appropriate W addition can significantly enhance the GFA of the $Fe_{47-x}Cr_{20}Mo_{10}W_xC_{15}B_6Y_2$ alloys.

The structure of the $Fe_{47-x}Cr_{20}Mo_{10}W_xC_{15}B_6Y_2$ alloys was further analyzed by TEM. Fig. 2 shows the high-resolution TEM (HRTEM) images and corresponding selected area electron diffraction (SAED, inset) patterns of the $Fe_{47-x}Cr_{20}Mo_{10}W_xC_{15}B_6Y_2$ alloys. The dark field TEM image in Fig. 2 (a) and SAED pattern in Fig. 2 (b) show that the nanocrystalline phases with a size of approximately 4–25 nm in the $Fe_{47}Cr_{20}Mo_{10}C_{15}B_6Y_2$ alloy sample with a diameter of 6 mm can be indexed as the $Fe_{23}B_6$ phase (PDF number 47-1332), which is consistent with the XRD result in Fig. 1.

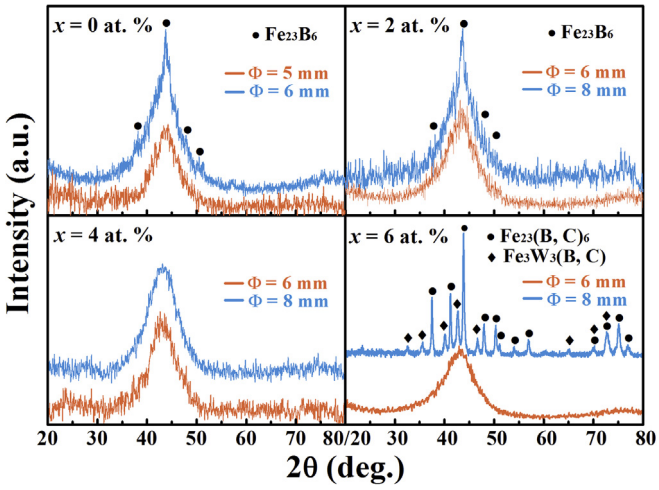

Fig. 1. XRD patterns of the as-cast $Fe_{47-x}Cr_{20}Mo_{10}W_xC_{15}B_6Y_2$ ($x = 0, 2, 4, 6$ at. %) alloys.

The SAED patterns of Fig. 2 (c), and (d) separately reveal a full ring, which is an inherent characteristic of the amorphous structure and confirms fully amorphous structures in the $Fe_{45}Cr_{20}Mo_{10}W_2C_{15}B_6Y_2$ ($\Phi = 6$ mm) and $Fe_{43}Cr_{20}Mo_{10}W_4C_{15}B_6Y_2$ ($\Phi = 8$ mm) alloys.

The XRD and TEM results show that the appropriate W addition exhibits a beneficial effect on the GFA in the $Fe_{47-x}Cr_{20}Mo_{10}W_xC_{15}B_6Y_2$ alloys. The metastable $Fe_{23}B_6$ phase can be significantly suppressed with the small W addition (2 at. %). A fully amorphous structure can be attained in the $Fe_{43}Cr_{20}Mo_{10}W_4C_{15}B_6Y_2$ alloy sample with a maximum diameter of 8 mm with the continual W addition to 4 at. %, the GFA significantly decreased due to the generation of crystals with the excessive W addition (6 at. %).

The DSC curves of $Fe_{47-x}Cr_{20}Mo_{10}W_xC_{15}B_6Y_2$ ($x = 0, 2, 4, 6$ at. %) alloy ribbons are presented in Fig. 3. All the curves show evident glass transition characters in the temperature range from 854 K to 881 K, followed by a supercooled liquid region, multiple-stage crystallizations (Fig. 3a), and melting within a temperature interval (Fig. 3b). The number of crystallization peaks increased with the W addition, indicating that W addition causes the formation of more competitive crystalline phases, increases the crystallization difficulty, and promotes the amorphous phase forming ability [27]. Meanwhile, the DSC trace of the $Fe_{43}Cr_{20}Mo_{10}W_4C_{15}B_6Y_2$ alloy shows relatively fewer melting peaks and smaller melting interval, which implies that the composition of this alloy is closer to the eutectic point of the multi-component system and leads to a higher GFA [17].

The parameters of the supercooled liquid region ΔT_x ($T_x - T_g$) [1] and criterion γ [$T_x/(T_g + T_l)$] [28] are employed as the GFA criteria to evaluate the GFA dependence on the W addition. Table 1 summarizes the corresponding thermal parameters for $Fe_{47-x}Cr_{20}Mo_{10}W_xC_{15}B_6Y_2$ ($x = 0, 2, 4, 6$ at. %) alloys and other typical Fe-based BMGs. The W addition can increase the glass transition temperature T_g, onset crystallization temperature T_x, and onset melting temperature T_m. W atom addition strengthens the cohesive

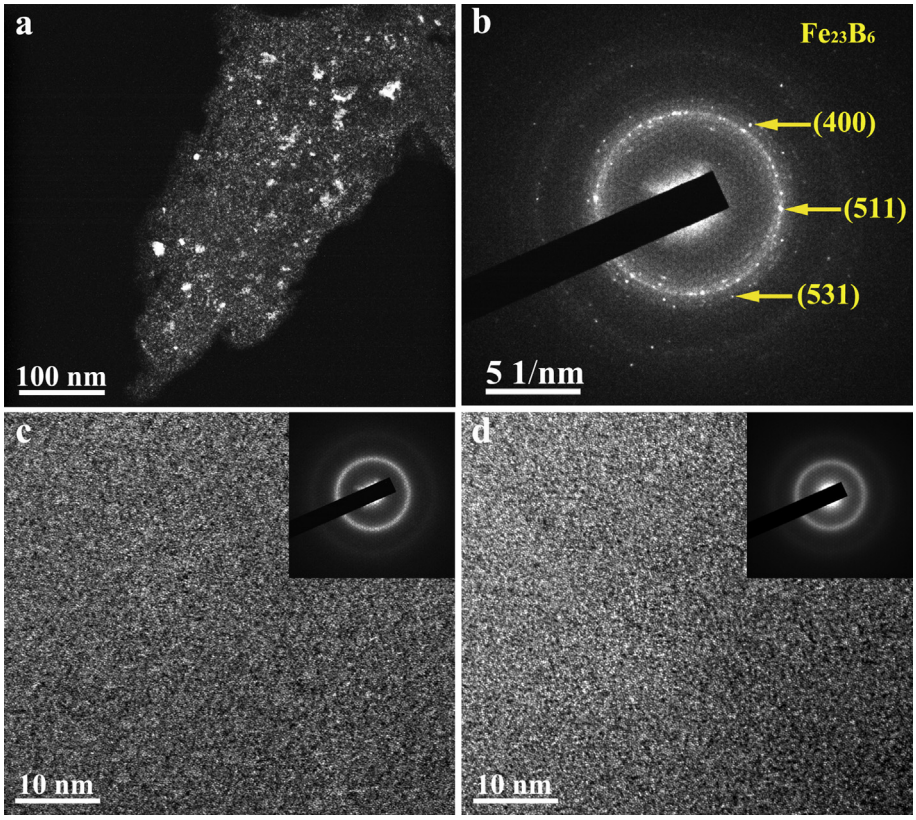

Fig. 2. The dark field TEM image (a) and SAED pattern (b) of 6 mm $Fe_{47}Cr_{20}Mo_{10}C_{15}B_6Y_2$ sample, HRTEM images and corresponding SAED patterns (inset) of 6 mm $Fe_{45}Cr_{20}Mo_{10}W_2C_{15}B_6Y_2$ sample (c) and 8 mm $Fe_{43}Cr_{20}Mo_{10}W_4C_{15}B_6Y_2$ sample (d).

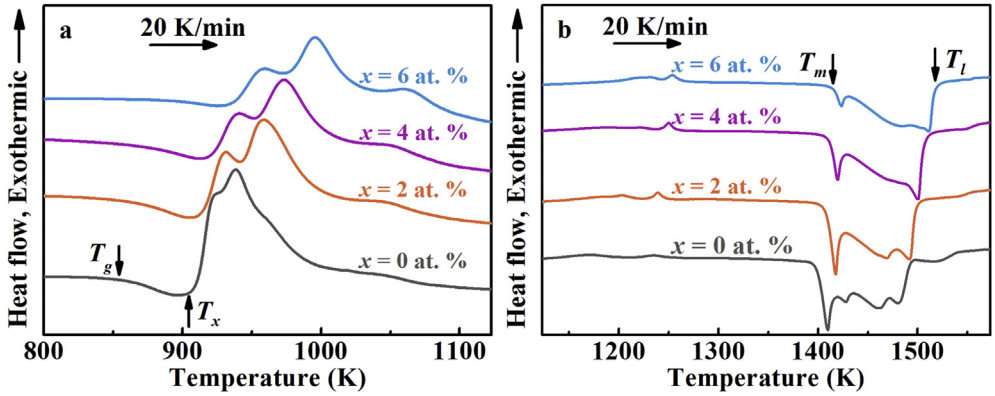

Fig. 3. DSC curves of $Fe_{47-x}Cr_{20}Mo_{10}W_xC_{15}B_6Y_2$ (x = 0, 2, 4, 6 at. %) ribbons, which show (a) glass transition, crystallization, and (b) melting events.

Table 1
Critical diameter (d_c), thermal stabilities and mechanical properties of $Fe_{47-x}Cr_{20}Mo_{10}W_xC_{15}B_6Y_2$ (x = 0, 2, 4, 6 at. %) and other typical Fe-based BMGs.

Alloy	d_c (mm)	Thermal Stability						Mechanical Property		Reference
		T_g (K)	T_x (K)	T_m (K)	T_l (K)	ΔT_x (K)	γ	Compressive Strength (GPa)	Hardness (HV)	
$Fe_{59}Cr_6Mo_{14}C_{15}B_6$	1.5	806	858	–	1436	52	0.383	4.40	–	[40]
$Fe_{48}Cr_{15}Mo_{14}C_{15}B_6Y_2$	9	848	–	–	1453	–	–	–	–	[11]
$Fe_{48}Cr_{15}Mo_{14}C_{15}B_6Er_2$	12	843	893	–	1443	50	0.391	4.20	–	[40]
$(Fe_{44.3}Cr_{10}Mo_{13.8}Mn_{11.2}C_{15.8}B_{5.9})_{98.5}Y_{1.5}$	12	836	–	1369	1440	–	–	–	1287	[14]
$Fe_{41}Co_7Cr_{15}Mo_{14}C_{15}B_6Y_2$	16	838	876	1387	1437	38	0.385	3.50	1253	[16]
$Fe_{47}Cr_{20}Mo_{10}C_{15}B_6Y_2$	5	854	909	1398	1494	55	0.387	3.53	1176	This Work
$Fe_{45}Cr_{20}Mo_{10}W_2C_{15}B_6Y_2$	6	856	913	1406	1500	57	0.388	3.85	1205	This Work
$Fe_{43}Cr_{20}Mo_{10}W_4C_{15}B_6Y_2$	8	858	920	1410	1503	62	0.390	3.99	1238	This Work
$Fe_{41}Cr_{20}Mo_{10}W_6C_{15}B_6Y_2$	6	881	918	1416	1518	37	0.383	4.12	1267	This Work

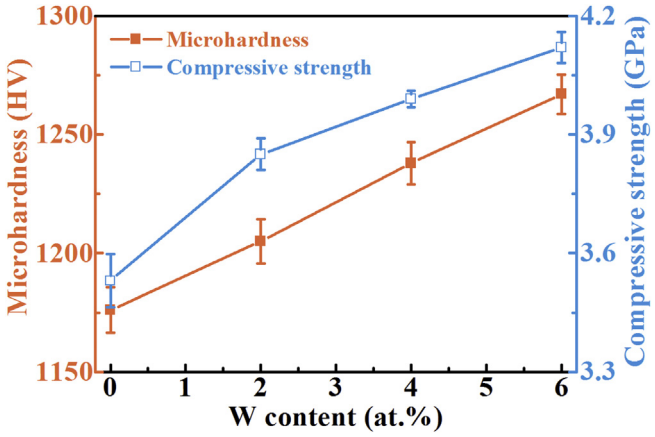

Fig. 4. Microhardness and compressive strength of the $Fe_{47-x}Cr_{20}Mo_{10}W_xC_{15}B_6Y_2$ BMGs.

energy through the formation of W-W, W-C and W-B bonds in Fe-based metallic glasses, and the high cohesive energy results in the increase in T_g, T_x and T_m [29]. Moreover, the $Fe_{43}Cr_{20}Mo_{10}W_4C_{15}B_6Y_2$ alloy shows the highest GFA criterion values (ΔT_x = 62 K and γ = 0.390, Table 1), indicating relatively higher stability against crystallization [30].

S. J. Poon et al. [31] proposed a network-like structure theory for Fe-based metallic glass. In the Fe-Cr-Mo-W-C-B-Y alloy system, the refractory atoms (e.g., Mo and W) and rare earth element (Y) prefer to occupy central positions in the atomic arrangement, whereas small atoms (B and C) are located at the interstitial positions. The large atoms and small atoms can form a reinforced "backbone" in the amorphous structure, which increases the atomic packing density. Thus, the atomic packing density of the $Fe_{47-x}Cr_{20}Mo_{10}W_xC_{15}B_6Y_2$ alloys increases with the appropriate W addition due to the radius differences among the Y (0.182 nm), W (0.137 nm), Mo (0.136 nm), Cr (0.125 nm), Fe (0.124 nm), B (0.090 nm), and C (0.077 nm) atoms. The negative mixing enthalpy of W-B (31 kJ/mol) and W-C (60 kJ/mol) are larger than that of Fe-B (26 kJ/mol) and Fe-C (50 kJ/mol), respectively [32]. The cohesive forces and confusion effect [25], which are induced by the addition of refractory W atoms, can cause denser atom packing in the liquid state that blocks the long-range atomic diffusion, hampers the nucleation of crystalline phases, and favors the formation of an amorphous phase [33].

However, increasing the W addition to 6 at. % engenders the atomic-scale chemical inhomogeneity due to the positive mixing enthalpy among constituent elements [25] (W-Y: 24 kJ/mol; Mo-Y: 24 kJ/mol; Cr-Y: 11 kJ/mol [32]), which in turn, triggers the nucleation of the $Fe_{23}(B, C)_6$ and $Fe_3W_3(B, C)$-type phases in Fe-based BMGs. This result is consistent with the Mo element addition in the Fe-Mo-P-C-B-Si alloy system [27,34]. The formation of $M_{23}(B, C)_6$-type phase with the long range network-like atomic configuration in the supercooled liquid in multi-component Fe-based BMG alloy system is considered as the origin for the high thermal stability and GFA [8].

The effects of W addition on the mechanical properties were evaluated by microhardness and uniaxial compression tests. As shown in Fig. 4, the mechanical properties of $Fe_{47-x}Cr_{20}Mo_{10}W_xC_{15}B_6Y_2$ (x = 0, 2, 4, 6 at. %) alloys are depend on the content of W element. The corresponding microhardness and compressive strength are given in Table 1. It can be seen that the microhardness and compressive strength increases from 1176 HV and 3.53 GPa for $Fe_{47}Cr_{20}Mo_{10}C_{15}B_6Y_2$ alloy to 1267 HV and 4.12 GPa for $Fe_{41}Cr_{20}Mo_{10}W_6C_{15}B_6Y_2$ alloy, respectively. The wear resistance is dependent on the material hardness (i.e., higher hardness indicates high wear resistance) [35]; thus, W addition also has a beneficial effect on wear resistance. Due to a larger atom size, W atom could enlarge the atomic size distribution in Fe-based BMG alloys, which results the enhancement of topological ordering and formation of a highly dense random packed structure, and thus leads to a higher fracture strength [36]. Besides, W addition increases the ratios of the W-W, W-C and W-B bonds; these bonds with high binding energy lead to the increased hardness and compressive strength [29,37].

Fe-based BMGs commonly have high strength with no plasticity. The fracture morphologies of the $Fe_{47}Cr_{20}Mo_{10}C_{15}B_6Y_2$ and $Fe_{45}Cr_{20}Mo_{10}W_2C_{15}B_6Y_2$ alloys were observed to explore the fracture mechanism of the $Fe_{47-x}Cr_{20}Mo_{10}W_xC_{15}B_6Y_2$ BMGs. A typical brittle cleavage rupture morphology, which consists of mirror-like regions and tear lines, is shown in Fig. 5 (a) for the $Fe_{47}Cr_{20}Mo_{10}C_{15}B_6Y_2$ alloy. No visible plastic deformation patterns are observed in the fracture surface of this alloy. Although no plastic elongation appears in the compression stress-strain curve of $Fe_{45}Cr_{20}Mo_{10}W_2C_{15}B_6Y_2$ alloy, some dimple and vein-like patterns are observed in Fig. 5 (b).

The toughness of Fe-based BMGs can be evaluated by indentation fracture toughness test [38]. Indentation cracking patterns can be observed around the corners of indent under a high indentation load, the crack geometry can be used to establish the indentation toughness values [39]. It was found that the fracture toughness (K_{IC}) of $Fe_{47-x}Cr_{20}Mo_{10}W_xC_{15}B_6Y_2$ alloys increased from 1.25 MPa $m^{1/2}$ (x = 0 at. %), 1.89 MPa $m^{1/2}$ (x = 2 at. %) to 2.05 MPa $m^{1/2}$ (x = 6 at. %). Instead of indentation cracks, shear bands were observed at the edges of indents in $Fe_{43}Cr_{20}Mo_{10}W_4C_{15}B_6Y_2$ alloy, it could be summarized that appreciate W addition can improve the toughness of Fe-based BMGs.

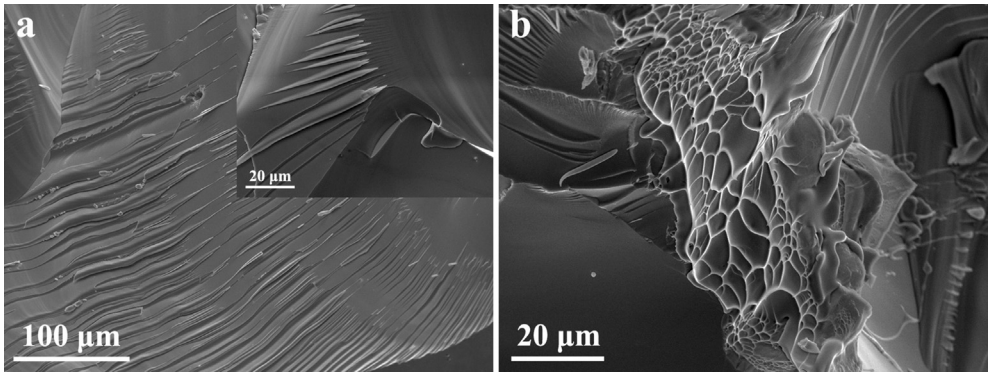

Fig. 5. Fracture morphology of as-cast glassy rods (Φ = 2 mm) after compressive tests on the (a) $Fe_{47}Cr_{20}Mo_{10}C_{15}B_6Y_2$ and (b) $Fe_{45}Cr_{20}Mo_{10}W_2C_{15}B_6Y_2$ BMGs.

4. Conclusions

The present study shows that the partial substitution of Fe by the W element can significantly enhance the GFA and thermal stabilities of $Fe_{47-x}Cr_{20}Mo_{10}W_xC_{15}B_6Y_2$ alloys through the inhibition of the formation of the $Fe_{23}B_6$ crystal. Fully amorphous $Fe_{43}Cr_{20}Mo_{10}W_4C_{15}B_6Y_2$ alloy rods with a maximum diameter of 8 mm can be fabricated through the copper mold casting with commercial purity materials by increasing the W content to 4 at. %. The GFA and thermal stability decreases when W addition exceeds 4 at. %. Moreover, the substitution of Fe by W can also affect the mechanical properties of $Fe_{47-x}Cr_{20}Mo_{10}W_xC_{15}B_6Y_2$ BMGs. The hardness, compressive strength and plasticity improves significantly with the increment in the W content from 0 at. % to 6 at. %. In addition, the microhardness and compression strength of the $Fe_{41}Cr_{20}Mo_{10}W_6C_{15}B_6Y_2$ BMG are as high as 1267 HV and 4.12 GPa, respectively.

Acknowledgments

This work is supported by National Key Research and Development Plan of China (Grant No. 2016YFB0300502), National Science Foundation of China (Grant No. 51601129) and Shanghai Pujiang Program (Grant No. 16PJ1410000).

References

[1] A. Inoue, Stabilization of metallic supercooled liquid and bulk amorphous alloys, Acta Mater. 48 (2000) 279–306.
[2] W.H. Wang, C. Dong, C.H. Shek, Bulk metallic glasses, Mater. Sci. Eng. R 44 (2004) 45–89.
[3] P.F. Gostin, A. Gebert, L. Schultz, Comparison of the corrosion of bulk amorphous steel with conventional steel, Corros. Sci. 52 (2010) 273–281.
[4] J. Eckert, J. Das, S. Pauly, C. Duhamel, Mechanical properties of bulk metallic glasses and composites, J. Mater. Res. 22 (2011) 285–301.
[5] X.Y. Fu, T. Kasai, M.L. Falk, D.A. Rigney, Sliding behavior of metallic glass: Part I. Experimental investigations, Wear 250 (2001) 409–419.
[6] X.Y. Fu, M.L. Falk, D.A. Rigney, Sliding behavior of metallic glass: Part II. Computer simulations, Wear 250 (2001) 420–430.
[7] Y.Z. Lu, Y.J. Huang, X. Lu, Z.X. Qin, J. Shen, Specific heat capacities of Fe-Co-Cr-Mo-C-B-Y bulk metallic glasses and their correlation with glass-forming ability, Mater. Lett. 143 (2015) 191–193.
[8] C. Suryanarayana, A. Inoue, Iron-based bulk metallic glasses, Int. Mater. Rev. 58 (2013) 131–166.
[9] W.H. Wang, Roles of minor additions in formation and properties of bulk metallic glasses, Prog. Mater. Sci. 52 (2007) 540–596.
[10] V. Ponnambalam, S.J. Poon, G.J. Shiflet, V.M. Keppens, R. Taylor, G. Petculescu, Synthesis of iron-based bulk metallic glasses as nonferromagnetic amorphous steel alloys, Appl. Phys. Lett. 83 (2003) 1131.
[11] V. Ponnambalam, S.J. Poon, G.J. Shiflet, Fe-based bulk metallic glasses with diameter thickness larger than one centimeter, J. Mater. Res. 19 (2004) 1320–1323.
[12] M. Siddique, M. Iqbal, J.I. Akhter, M. Ahmad, Crystallization and phase identification of $Fe_{50}Cr_{14}Mo_{14}C_{14}B_6X_2$ bulk amorphous steels by Mössbauer spectroscopy, J. Alloys Compd. 482 (2009) L25–L28.
[13] J. Pan, Q. Chen, N. Li, L. Liu, Formation of centimeter Fe-based bulk metallic glasses in low vacuum environment, J. Alloys Compd. 463 (2008) 246–249.
[14] Z.P. Lu, C.T. Liu, J.R. Thompson, W.D. Porter, Structural amorphous steels, Phys. Rev. Lett. 92 (2004) 245503.
[15] K. Amiya, A. Inoue, Fe-(Cr,Mo)-(C,B)-Tm bulk metallic glasses with high strength and high glass-forming ability, Mater. Trans. 47 (2006) 1615–1618.
[16] J. Shen, Q.J. Chen, J.F. Sun, H.B. Fan, G. Wang, Exceptionally high glass-forming ability of an FeCoCrMoCBY alloy, Appl. Phys. Lett. 86 (2005) 151907.
[17] Q.J. Chen, D.L. Zhang, J. Shen, H.B. Fan, J.F. Sun, Effect of yttrium on the glass-forming ability of Fe-Cr-Mo-C-B bulk amorphous alloys, J. Alloys Compd. 427 (2007) 190–193.
[18] A. Inoue, T. Zhang, H. Koshiba, A. Makino, New bulk amorphous Fe-(Co, Ni)-M-B (M = Zr, Hf, Nb, Ta, Mo, W) alloys with good soft magnetic properties, J. Appl. Phys. 83 (1998) 6326.
[19] X.H. Yang, X.H. Ma, Q. Li, S.F. Guo, The effect of Mo on the glass forming ability, mechanical and magnetic properties of FePC ternary bulk metallic glasses, J. Alloys Compd. 554 (2013) 446–449.
[20] X. Li, C.L. Qin, H. Kato, A. Makino, A. Inoue, Mo microalloying effect on the glass-forming ability, magnetic, mechanical and corrosion properties of $(Fe_{0.76}Si_{0.096}B_{0.084}P_{0.06})_{100-x}Mo_x$ bulk glassy alloys, J. Alloys Compd. 509 (2011) 7688–7691.
[21] F.Q. Zhai, E. Pineda, M.J. Duarte, D. Crespo, Role of Nb in glass formation of Fe-Cr-Mo-C-B-Nb BMGs, J. Alloys Compd. 604 (2014) 157–163.
[22] M.G. Nabiałek, M.J. Dośpiał, M. Szota, P. Pietrusiewicz, J. Jędryka, Investigation of the thermal and magnetic properties of $Fe_{61}Co_{10}Zr_{2.5}Hf_{2.5}Me_2W_2B_{20}$ (Me = Y, Nb, W, Ti, Mo, Ni) bulk amorphous alloys obtained by an induction suction method, J. Alloys Compd. 509 (2011) 3382–3386.
[23] L.Q. Ma, L. Wang, T. Zhang, A. Inoue, Effect of Nb addition on glass-forming ability, strength, and hardness of Fe-B-Zr amorphous alloys, Mater. Res. Bull. 34 (1999) 915–920.
[24] I. Kucuk, M. Aykol, O. Uzun, M. Yildirim, M. Kabaer, N. Duman, F. Yilmaz, K. Erturk, M.V. Akdeniz, A.O. Mekhrabov, Effect of (Mo, W) substitution for Nb on glass forming ability and magnetic properties of Fe-Co-based bulk amorphous alloys fabricated by centrifugal casting, J. Alloys Compd. 509 (2011) 2334–2337.
[25] X.M. Huang, C.T. Chang, Z.Y. Chang, A. Inoue, J.Z. Jiang, Glass forming ability, mechanical and magnetic properties in Fe-W-Y-B alloys, Mater. Sci. Eng. A 527 (2010) 1952–1956.
[26] A.A. Novakova, G.V. Sidorova, T.Y. Kiseleva, A. Szasz, Crystallization study of amorphous system $Fe_{84-x}W_xB_{16}$ (x = 3; 5), Hyperfine Interact. 73 (1992) 309–312.
[27] B.L. Shen, M. Akiba, A. Inoue, Effects of Si and Mo additions on glass-forming in FeGaPCB bulk glassy alloys with high saturation magnetization, Phys. Rev. B 73 (2006) 104204.
[28] Z.P. Lu, C.T. Liu, A new glass-forming ability criterion for bulk metallic glasses, Acta Mater. 50 (2002) 3501–3512.
[29] P. Öztürk, A. Hitit, Effects of tungsten and boron contents on crystallization temperature and microhardness of tungsten based metallic glasses, Acta Metall. Sin. 28 (2015) 733–738.
[30] Z.P. Lu, C.T. Liu, Glass formation criterion for various glass-forming systems, Phys. Rev. Lett. 91 (2003) 115505.
[31] S.J. Poon, G.J. Shiflet, F.Q. Guo, V. Ponnambalam, Glass formability of ferrous- and aluminum-based structural metallic alloys, J. Non Cryst. Solids 317 (2003) 1–9.
[32] A. Takeuchi, A. Inoue, Classification of bulk metallic glasses by atomic size difference, heat of mixing and period of constituent elements and its application to characterization of the main alloying element, Mater. Trans. 46 (2005) 2817–2829.
[33] Q. Yu, X.D. Wang, H.B. Lou, Q.P. Cao, J.Z. Jiang, Atomic packing in Fe-based metallic glasses, Acta Mater. 102 (2016) 116–124.
[34] B.L. Shen, M. Akiba, A. Inoue, Excellent soft-ferromagnetic bulk glassy alloys with high saturation magnetization, Appl. Phys. Lett. 88 (2006) 131907.
[35] T. Gloriant, Microhardness and abrasive wear resistance of metallic glasses and nanostructured composite materials, J. Non Cryst. Solids 316 (2003) 96–103.
[36] Z. Jiao, H. Li, J. Gao, Y. Wu, Z. Lu, Effects of alloying elements on glass formation, mechanical and soft-magnetic properties of Fe-based metallic glasses, Intermetallics 19 (2011) 1502–1508.
[37] A. Inoue, B.L. Shen, C.T. Chang, Super-high strength of over 4000 MPa for Fe-based bulk glassy alloys in $[(Fe_{1-x}Co_x)_{0.75}B_{0.2}Si_{0.05}]_{96}Nb_4$ system, Acta Mater. 52 (2004) 4093–4099.
[38] A.G. EVans, E.A. Charles, Fracture toughness determinations by indentation, J. Am. Ceram. Soc. 59 (1976) 371–372.
[39] P.A. Hess, S.J. Poon, G.J. Shiflet, R.H. Dauskardt, Indentation fracture toughness of amorphous steel, J. Mater. Res. 20 (2011) 783–786.
[40] X.J. Gu, S.J. Poon, G.J. Shiflet, Mechanical properties of iron-based bulk metallic glasses, J. Mater. Res. 22 (2011) 344–351.